

Designing transparent conductors using forbidden optical transitions

Rachel Woods-Robinson^{1,2}, Yihuang Xiong³, Jimmy-Xuan Shen⁴, Nicholas Winner^{1,6}, Matthew K. Horton¹, Mark Asta^{1,6}, Alex M. Ganose⁵, Geoffroy Hautier³, and Kristin A. Persson^{6,7}

¹Materials Sciences Division, Lawrence Berkeley National Laboratory, Berkeley, CA, USA, ²Applied Science and Technology Graduate Group, University of California at Berkeley, Berkeley, CA, USA,

³Thayer School of Engineering, Dartmouth College, 14 Engineering Dr, Hanover, NH, USA, ⁴Lawrence Livermore National Laboratory,

Livermore, CA, USA, ⁵Department of Chemistry, Molecular Sciences Research Hub, White City Campus, Imperial College London, Wood Lane, London, UK,

⁶Department of Materials Science and Engineering, University of California at Berkeley, Berkeley, CA, USA, ⁷Molecular Foundry Division, Lawrence Berkeley National Laboratory, Berkeley, CA, USA,

(Dated: April 11, 2023)

Many semiconductors present weak or forbidden transitions at their fundamental band gaps, inducing a widened region of transparency. This occurs in high-performing n-type transparent conductors (TCs) such as Sn-doped In₂O₃ (ITO), however thus far the presence of forbidden transitions has been neglected in searches for new p-type TCs. To address this, we first compute high-throughput absorption spectra across ~18,000 semiconductors, showing that over half exhibit forbidden or weak optical transitions at their band edges. Next, we demonstrate that compounds with highly localized band edge states are more likely to present forbidden transitions. Lastly, we search this set for p-type and n-type TCs with forbidden or weak transitions. Defect calculations yield unexplored TC candidates such as ambipolar BeSiP₂, Zr₂Sn₂ and KSe, p-type BAs, Au₂S, and AuCl, and n-type Ba₂InGaO₅, GaSbO₄, and KSbO₃, among others. We share our data set via the MPContribs platform, and we recommend that future screenings for optical properties use metrics representative of absorption features rather than band gap alone.

INTRODUCTION

It is often assumed in semiconductors that a strong absorption onset occurs at the direct fundamental band gap. This is indeed the case for many materials, however some materials have forbidden transitions at their band edges such that the onset of their absorption edge occurs at higher energies than their direct gap. Four scenarios of absorption in semiconductors are depicted schematically in **Figure 1**, following the optical type (OT) classification as outlined by Yu and Zunger[1] for four hypothetical materials with similar band structures. In OT1 the fundamental band gap E_G is direct and allowed (“da”), in OT2 E_G is direct but forbidden (“df”), in OT3 E_G is indirect and the direct gap is allowed (“ia”), and in OT4 E_G is indirect and the direct gap is forbidden (“if”).

The presence of forbidden optical transitions can be detrimental in certain applications (e.g., LEDs, solar cell absorbers), however for others it may present a useful design criteria. In this study we focus on transparent conductors (TCs) — materials combining wide optical transparency with high mobility and doping — which require weak absorption within a given range of wavelengths (usually within the visible) such that forbidden transitions could be advantageous to increase transparency. In fact, many of the high-performing, commercially-available n-type transparent conducting oxides (TCOs) have dipole forbidden transitions at their band edges that induce this behavior. A notable example occurs in the most common TCO, n-type Sn-doped In₂O₃ (ITO), with weak absorption in the upper-most 0.8 eV of the valence band (VB),

allowing for an increased transparency in addition to the increase from the Burstein-Moss effect.[2] Other wide-gap oxide materials with reported forbidden transitions include SnO₂ and F-doped SnO₂ (FTO),[3, 4] spinels SnZn₂O₄, SnCd₂O₄ and CdIn₂O₄,[5] Ti₂O₃,[6] and TiO₂.[7] Additionally, dipole-forbidden transitions have been reported in Cu-based p-type TCs including delafossites CuAlO₂, CuGaO₂, and CuInO₂, as well as cuprite Cu₂O.[8]

Meanwhile, it is of considerable interest to identify new high-performing p-type TC for applications in photovoltaics and beyond. Over the past decade, high-throughput screening studies have proposed several n-type or p-type TC candidates such as ZnSb₂O₆, ZrOS, BP, Ba₂BiTaO₆, and CaTe[9–13]. Experimental confirmation of exceptional properties has been demonstrated in some of those computationally-identified materials such as the p-type Ba₂BiTaO₆ and n-type ZnSb₂O₆,[11, 14] but still no predicted p-type TC has experimentally-confirmed properties on par with n-type ITO. Most high-throughput screenings for TCs to date assume wide electronic band gap or direct band gap as a proxy for transparency.[9, 12, 15–18] This assumption does not consider whether associated optical transitions are actually allowed or strong, thus overlooking materials with a small fundamental band gap but a wide absorption edge which could enable optical transparency. We note that several screenings for solar absorbers have explicitly considered forbidden transitions,[1, 19, 20] *excluding* materials with forbidden edges to design for a sharp absorption onset; in contrast, a screening for TCs would *include* such materials.

Therefore, in this work we leverage forbidden optical

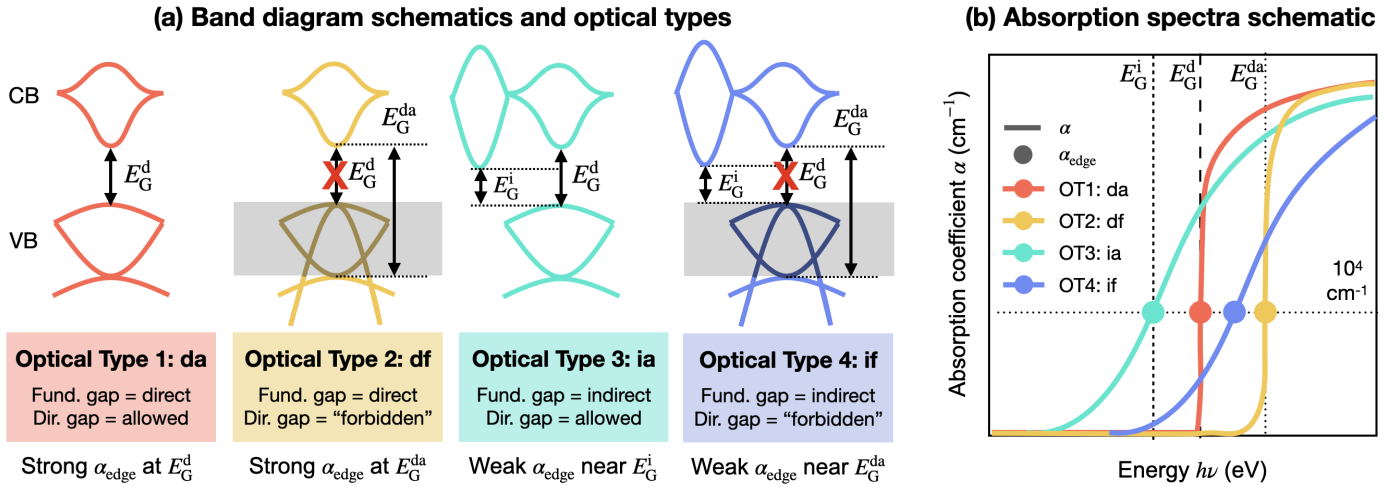


Figure 1: (a) Band schematics and (b) cartoon of the resulting absorption spectra of the four optical types (OTs) in semiconductor materials. Band schematics on left are inspired by Yu and Zunger.[1] The grey regions in OT2 and OT4 correspond to the forbidden region where transitions do not occur. “Fund. gap” stands for fundamental electronic band gap and “dir. gap” stands for direct band gap.

transitions at band edges (referred to hereafter as simply “forbidden transitions”) to improve high-throughput searches for TCs. First, we benchmark and compute optical absorption edges for $\sim 18,000$ inorganic compounds in the Materials Project (MP) database, and classify optical types across MP to assess whether the fundamental gaps are optically allowed or forbidden. We show that over half of the selected semiconductors in MP exhibit a weak absorption edge, and that, in special cases involving transitions between localized states, the presence of forbidden transitions can be explained by orbital character. With this data, we introduce a series of high-throughput descriptors for p-type TCs to estimate the direct allowed band gap (often referred to in the literature as the “optical gap”), absorption edge onset, and average absorption spectra in the visible spectrum. Using these descriptors, we perform a high-throughput screening (as outlined in **Figure 2**) for promising p-type and n-type TCs with disperse band edges that may be transparent in the visible regime. Such compounds have low fundamental band gaps, and therefore may have previously been overlooked. To assess dopability and mobility for materials with good computed optical properties, we perform defect formation energy calculations and compute transport properties for the most promising candidates. We highlight some ambipolar TC candidates including BeSiP_2 , p-type TC candidates including boron BAs, and n-type TC candidates including barium indium gallium oxide ($\text{Ba}_2\text{InGaO}_5$), and share our data for further exploration.

MATERIALS AND METHODS

Density functional theory (DFT) calculations were performed using the projector augmented wave (PAW) method[45, 46] as implemented in the Vienna *Ab Initio* Simulation Package (VASP)[47, 48], first within the Perdew-Burke-Ernzerhof (PBE) Generalized Gradi-

ent Approximation (GGA) formulation of the exchange-correlation functional.[49] Cutoff, convergence, and correction criteria have been benchmarked and are used throughout the MP infrastructure, as described elsewhere.[50, 51] Effective mass (m^*) was computed from GGA calculations using the BoltzTraP2 package,[52] assuming dopings of 10^{18} cm⁻³ as described in the Supplementary Materials (SM). The HSE06 screened hybrid functional[53] was used to calculate gap corrections and apply scissor shifts in “screen 2.” Branch point energy (BPE) was computed from GGA calculations with an HSE gap correction; BPE ratio range σ_{BPE} was computed by varying number of valence bands (N_{VB}) and number of conduction bands (N_{CB}) from $N_{\text{VB}}:N_{\text{CB}}=2:4$ to $N_{\text{CB}}:N_{\text{CB}}=8:4$, with details described elsewhere.[25] The site-projected wave function character of orbitals at the band edges were assessed to compute the inverse participation ratios (IPRs) and the orbital overlaps (see SM).

Optical absorption coefficients were calculated with VASP using the independent-particle approximation (IPA). Using the IPA, the dielectric matrix elements are calculated using a k-point reciprocal density of $1,000 \text{ \AA}^{-3}$, which we have benchmarked and optimized for high-throughput screenings E_{edge} (for optimization of precision in the extended absorption spectrum, see Yang et al.[54]). Cutoff for a transition to be considered “allowed” was selected following convention from Fabini et al.[20] Details and calculation parameters for this method are reported in the SM.

Focusing on compounds that are likely to be synthesizable and are tractable for further defect calculations, we “pre-screen” (see Figure 2) the MP database using a series of filters. We include compounds in which the MP computed GGA fundamental band gap (E_G) is greater than 0.5 eV and the energy above convex hull (E_{hull}) is less than 0.1 eV/atom.[55, 56] Large compounds were filtered out with more than 5 elements or more than 12 symmetrically inequivalent sites (see `pymatgen.symmetry.analyzer`).

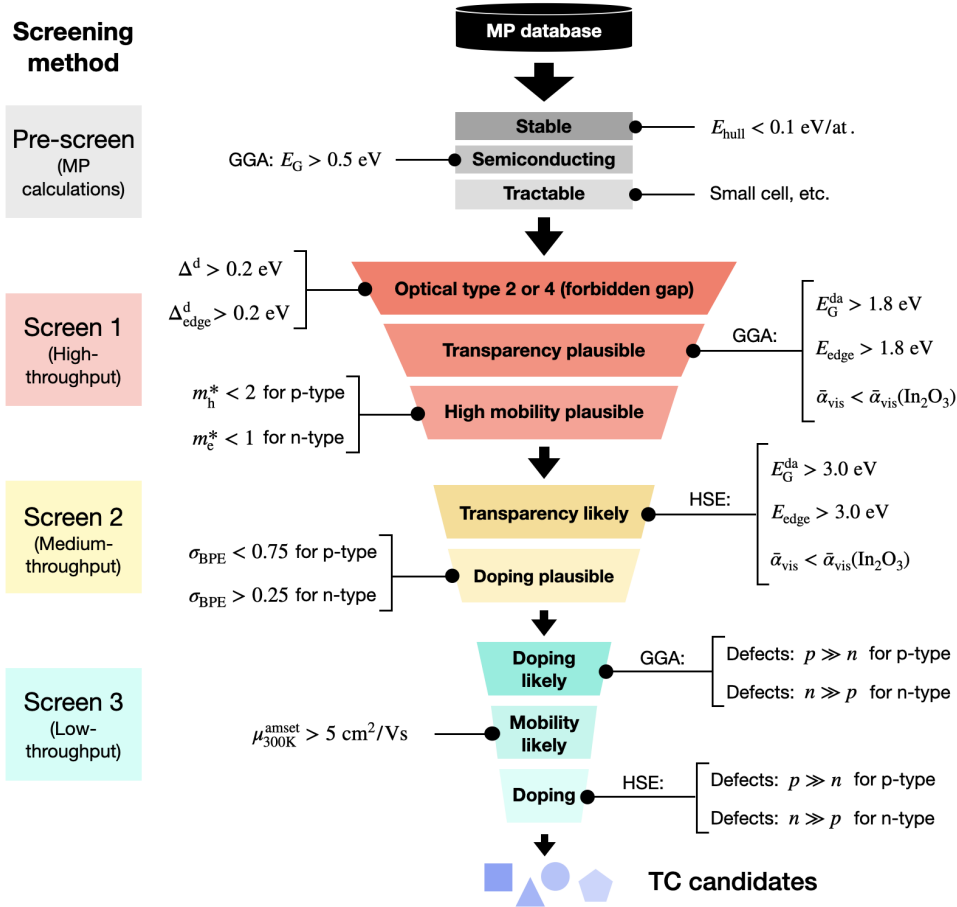


Figure 2: (a) The screening method for TCs pursued in this paper, focusing on compounds from the MP database with forbidden optical transitions. The targeted property is listed in the screen, and the descriptor and cutoff value are given on the right-hand side. Note that these descriptors are computed with both GGA (for screen 1) and HSE06 (for screen 2) functionals, and are described in more detail in the manuscript.

Compounds with heavy elements ($Z > 82$) and f-block elements are also filtered out (except for La). GGA absorption spectra of ~ 800 MP compounds from Fabini et al.’s search for PV absorber materials are publicly available on MPContribs and included in our set.[20, 57]

For compounds that emerge from “screen 2,” defect formation energy calculations are performed using the `pycdt` package,[58]. Hybrid density functional theory calculations of defect formation energies are performed using the CP2K software package and HSE06 functional.[53, 59, 60] Charge-carrier mobility is calculated using the *ab initio* scattering and transport package (`amset`),[38] which solves the linearized Boltzmann transport equation under the constant relaxation time approximation. Details for each of these methods are described in the SM.

RESULTS

Forbidden or weak transitions are common

As a result of the pre-screening, we obtain a data set of $\sim 18,000$ semiconductors compounds for which optical

absorption spectra and descriptors are assembled. Statistics and corresponding descriptors are summarized in **Figure 3**, grouped by optical type. We first assess the distribution of optical types (OTs) and forbidden optical transitions across the set. To our knowledge, this has not been assessed across known semiconductor materials, except for the several hundred from Fabini et al.[20] Figure 3(a) plots a histogram of the descriptor “forbidden energy difference” Δ^d , defined as:

$$\Delta^d = E_G^{\text{da}} - E_G^{\text{d}}, \quad (1)$$

where the direct allowed band gap E_G^{da} is defined as the energy at which dipole transition matrix elements become significant (adopting what constitutes as “significant” from the literature;[20] see Supplementary Materials, SM). We demonstrate that nearly 50% of compounds have forbidden transitions (i.e., $\Delta^d > 0$ eV) at the band edges. A large subset show a strong impact of forbidden transitions, $\sim 18\%$ with $\Delta^d > 0.2$ eV and 7% with $\Delta^d > 0.5$ eV. It is observed that OT3 (indirect gap, allowed direct transition) is the most common optical type, followed closely by OT4 (indirect fundamental gap, forbidden direct transition).

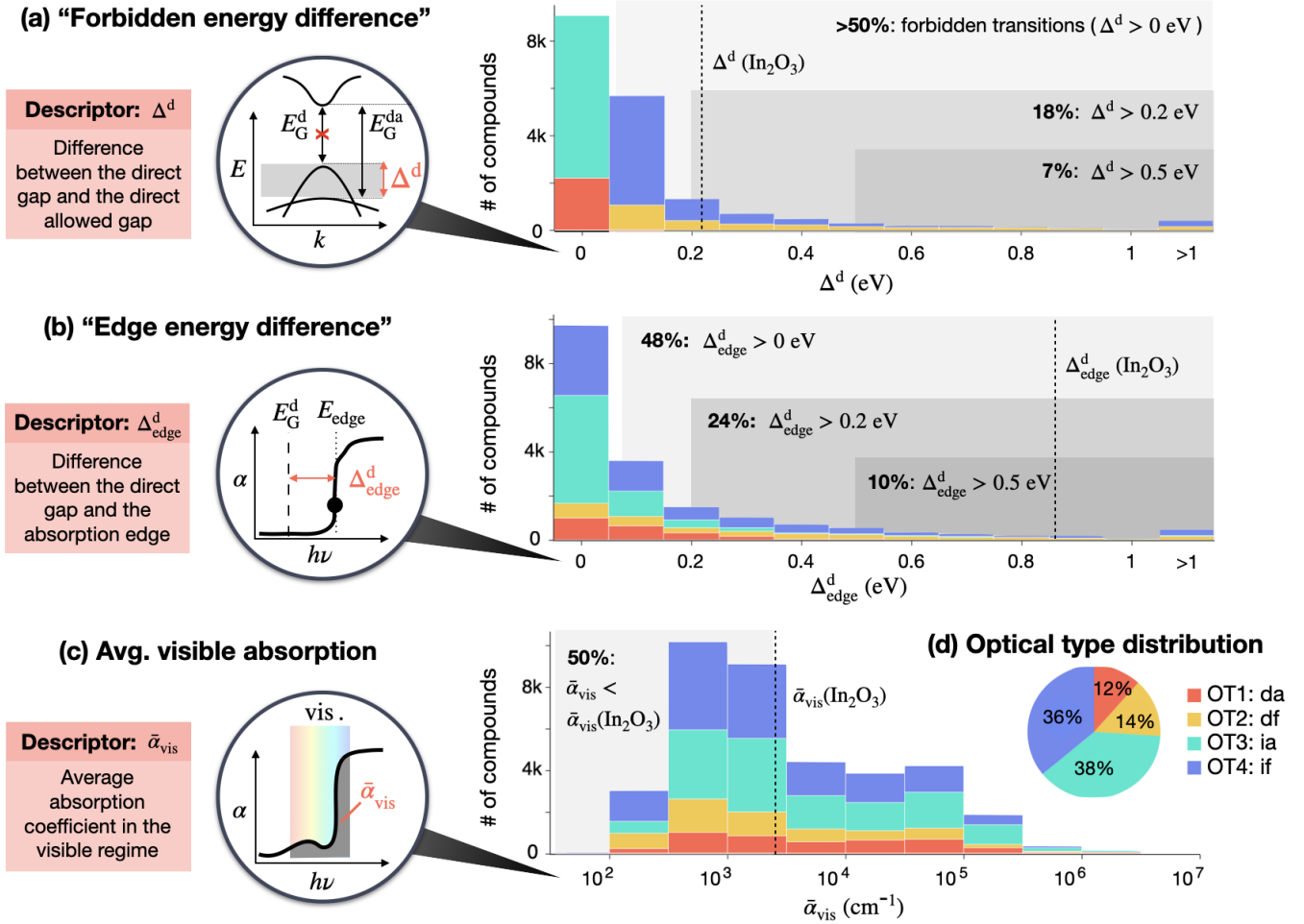


Figure 3: (Left) Schematics highlighting new optical screening descriptors: (a) “forbidden energy difference” Δ^d , (b) edge energy difference Δ^d_{edge} , and (c) average absorption in the visible regime $\bar{\alpha}_{\text{vis}}$. (Right) Histograms of these three optical descriptors are reported across the set of 18,000 semiconductors. Corresponding values for In_2O_3 , the best performing n-type TC, are denoted for reference. (d) Optical type (OT) distribution, showing over half of this set has a forbidden direct optical transition, 18% exhibit $\Delta^d > 0.2$ eV, and 7% exhibit $\Delta^d > 0.5$ eV.

Figure 3(b) reports the distribution of the “edge energy difference” Δ^d_{edge} , defined as:

$$\Delta^d_{\text{edge}} = E_{\text{edge}} - E_G^d, \quad (2)$$

where the absorption edge energy (E_{edge}) is defined as the energy at which the GGA IPA absorption coefficient exceeds 10^4 cm^{-1} (see SM). Some materials may have transitions at the band edges that are “allowed” but are only weakly absorbing; in these cases E_{edge} can provide a better metric than E_G^{da} for where the strong edge onset actually occurs. For example, in In_2O_3 (dashed lines) our computed Δ^d_{edge} of 0.68 eV corresponds better to the literature-reported Δ^d than our computed GGA Δ^d of 0.22 eV. Third, in Figure 3(c) we plot the distribution of the average absorption in the visible, $\bar{\alpha}_{\text{vis}}$, defined as:

$$\bar{\alpha}_{\text{vis}} = \int_{\nu_{\text{vis}}^{\text{min}}}^{\nu_{\text{vis}}^{\text{max}}} \alpha(h\nu), \quad (3)$$

i.e., the integral of the absorption spectra across the visible regime. Since GGA Kohn-Sham gap underestimates

fundamental band gap, we define the limits of the integral for GGA calculations using an empirical gap correction from Morales et al. (see SM).[21] It is observed that in more than 50% of compounds, $\bar{\alpha}_{\text{vis}}$ is less than that of In_2O_3 . Of interest to this study are the set of compounds with a significantly widened absorption edge due to forbidden transitions and correspondingly low absorption coefficients. In particular, we are interested in materials in which forbidden transitions raise the absorption edge outside of the visible spectrum and lead to optical transparency. However we note this data set may be valuable for other investigations as well.

Underlying chemical trends

Forbidden and weak optical transitions in semiconductors can arise from a variety of physical, structural, and chemical phenomena. Inversion symmetry at the band extrema can induce parity forbidden dipole transitions,[22] and a series of selection rules determine whether transitions can occur between states of different irreducible

representation. Parity-forbidden transitions are invoked, e.g., for In_2O_3 , among other materials, to explain in part why experimental optical band gaps exceed the fundamental gap. According to Fermi’s Golden Rule, if symmetry allows, transitions between localized states composed of similar chemical orbitals (i.e., with significant $\langle\psi_i|r|\psi_f\rangle$, which scales with overlap $\langle\psi_i|\psi_f\rangle$) have weak dipole transition matrix elements.[22] However, due to the delocalized nature of wavefunctions in solids, understanding the mechanisms behind forbidden and allowed transitions is less straightforward in semiconductors than in molecules with discrete, localized states.

Here, we explore whether the nature of forbidden transitions between the direct band edges can be correlated with two simple orbital-based descriptors, described in **Figure 5**:

- 1. Inverse participation ratio of the direct VBM and CBM states, $t_{\text{IPR}}^{\text{d}}$:** We consider the inverse participation ratio (IPR) across all compounds as a proxy for localization of states at the band edges (a high IPR indicates strong localization). As shown in Figure 5(a), “D” indicates a delocalized state and “L” indicates a localized state, and values of descriptor $t_{\text{IPR}}^{\text{d}}$ are assigned as shown in the call-out circle (e.g., $t_{\text{IPR}}^{\text{d}} = \text{“L}\rightarrow\text{L”}$ indicates a transition from a strongly localized VBM to a strongly localized CBM).
- 2. Orbital overlap of the direct VBM and CBM states, σ^{d} :** For each compound, we consider the dominant contributors to the density of states at the direct VBM and CBM, $\sigma(l, m)^{\text{d}}$ (l is angular momentum quantum number $s, p, d,$ or f for each element, and m is magnetic quantum number; see SM for details). With this data, we compute a descriptor σ^{d} (i.e., $\langle\psi_i|r|\psi_f\rangle$) to describe the similarity of CB edge and VB edge orbital contributions. This is depicted in the call-out circle in Figure 5(b) as:

$$\sigma^{\text{d}} = \sum_{l,m} \sigma(l, m)_{\text{VBM}}^{\text{d}} \sigma(l, m)_{\text{CBM}}^{\text{d}} \quad (4)$$

We will refer to this descriptor as “orbital overlap” in this paper.

Basic trends between these descriptors and the forbidden nature of the gap are summarized in Figure 5. In the violin plot in (a), it is shown that in compounds in which states at both band edges are delocalized (D→D), the forbidden energy difference Δ^{d} is low with a mean close to zero. In compounds where at least one band edge is delocalized (D→L and L→D), the average Δ^{d} increases slightly. However, compounds where both edges are highly localized (L→L) are significantly more likely to have wide forbidden transitions; the average Δ^{d} across such compounds is ~ 0.5 eV, and quartiles range from 0.1–0.6 eV. Therefore, transitions between two highly localized states are likely to lead to a forbidden transition.

To inspect cases with localized transitions in more detail, we compute the orbital overlap σ^{d} for the L→L subset from (a), and report the distribution of σ^{d} across the four optical types in the violin plot in Figure 5(b). It is observed that, systematically, compounds with allowed edges (OT1 and OT3) have significantly lower orbital overlaps than compounds with forbidden edges (OT2 and OT4). This is consistent with Fermi’s Golden Rule: low transition dipole matrix elements (i.e., forbidden or weak transitions) should occur between localized states with similar orbital contributions. We note that a weaker trend occurs when σ^{d} is plotted across all compounds (see SM), mostly likely because the selection rules from Fermi’s Golden Rule break down in transitions between delocalized states.

Therefore, in cases with highly localized band edges, σ^{d} is a useful predictor for the origin of forbidden transitions. However, these L→L cases are only a small subset ($\sim 10\%$) of compounds in which we predict forbidden transitions, and there are other factors that arise for example due to the delocalized or hybridized nature of edge states. Ultimately, due to the relatively cheap computational cost of high-throughput IPA calculations and the variety of mechanisms contributing to optical transition matrix elements, we recommend further DFT calculations at this stage.

Screening for TCs with forbidden transitions

Using this data set, we perform a high-throughput screening for transparent conductors with forbidden optical transitions at the band edges, which may have been excluded from previous screenings. We assess candidates for both p-type and n-type TCs. Our basic screening methodology is depicted in Figure 2(a). We note that the pre-screening steps restrict compounds to those with $E_{\text{hull}} < 0.1$ eV/atom as a proxy for stability, and to those with 12 or fewer symmetrically equivalent sites to allow for subsequent hybrid and defect calculations.

Screen 1: High-throughput absorption calculations

In screen 1 we filter compounds based on high-throughput GGA optical absorption calculations and corresponding effective masses at the band edges, as shown in the red-colored screening steps of Figure 2(a). Rather than considering the fundamental band gap E_{G} or direct band gap E_{G}^{d} , as done in previous screenings for p-type TCs,[9–13, 15–18] materials are filtered by either their direct allowed gap E_{G}^{da} , the onset of the absorption edge E_{edge} , or the average absorption coefficient in the visible $\bar{\alpha}_{\text{vis}}$. Schematics of these descriptors are depicted in Figure 2(b). We also prioritize compounds with large Δ^{d} or $\Delta_{\text{edge}}^{\text{d}}$, which indicate whether there is a strong presence of optically forbidden transitions at the band edges that could lead to a widening of the absorption edge.

In **Figure 4**(a) and (b), the effective mass m^* is plotted as a function of a GGA energy edge descriptor, either E_{G}^{da} or E_{edge} , depending on which value is higher. We

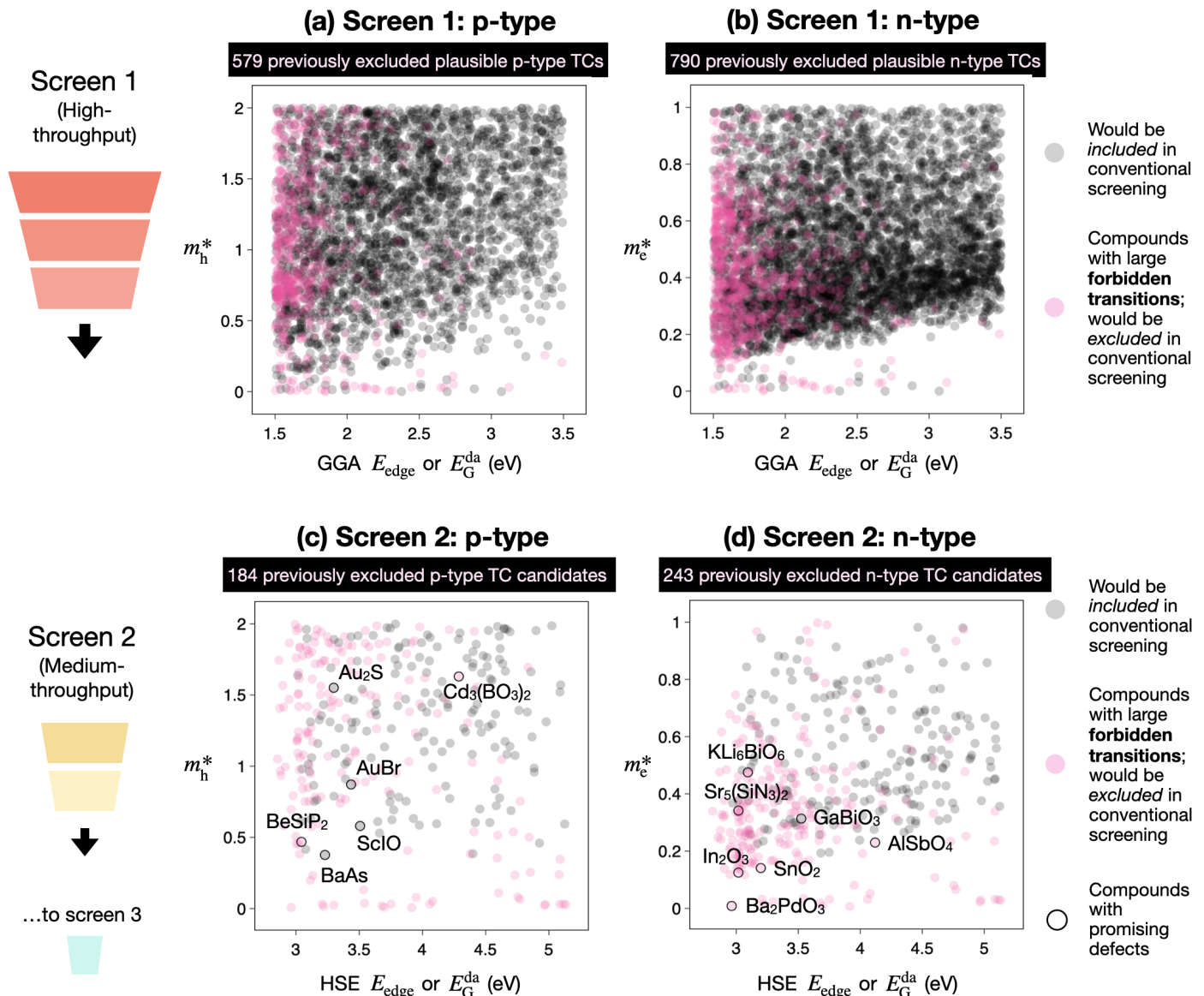


Figure 4: Screen 1 outputs using a GGA functional for (a) plausible p-type TC candidates (focusing on $m_h^* < 2$) and (b) plausible n-type TC candidates (focusing on $m_e^* < 1$). Screen 2 outputs using a HSE functional for (c) p-type TC candidates (focusing on $m_h^* < 2$) and (d) plausible n-type TC candidates (focusing on $m_e^* < 1$). In all four plots, computed m^* is plotted as a function of either E_G^{da} or E_{edge} , depending on which value is higher, to reflect the screening procedure. Marker color denotes whether compounds would have been included (blue) or excluded (red) from a conventional screening in which the allowed or forbidden nature of the direct gap is not considered. Candidates emerging from screen 3 are highlighted in (c) and (d).

restrict our screen to compounds with the GGA energy edge descriptor within the range of 1.5–3.2 eV. Note that for transparency in the visible, absorption edges greater than 3.0 eV are desirable, however PBE can underestimate band gap by a factor of ~ 1 –2 (depending on chemistry and structure)[24] hence the cutoff is reduced by a factor of two. We also include compounds in which the average absorption coefficient $\bar{\alpha}_{\text{vis}}$ is less than that of reference compound In_2O_3 ($2.7 \times 10^3 \text{ cm}^{-1}$ using the GGA functional). In this case, even if a material’s absorption edge occurs below 1.5 eV, if its total absorption is low enough we still include it in the screen. For the n-type TC screening, we restrict m_e^* to less than 1, however this tolerance is loosened to $m_h^* < 2$ for the p-type TC screening to reflect the much smaller

distribution of low m_h^* than low m_e^* across materials.[9, 25]

Figure 4(a) and (b) plot candidates emerging from screen 1. Pink-colored markers correspond to compounds with large forbidden transitions that would have likely been excluded from previous screens: 579 disperse valence band compounds (plausible p-type TCs) and 790 disperse conduction band compounds (plausible n-type TCs). In total, this amounts to 854 compounds, since most low m_h^* materials also exhibit low m_e^* . Grey-colored markers correspond to other materials within this range with small or no Δ^{d} , and these amount to 5,209 compounds.

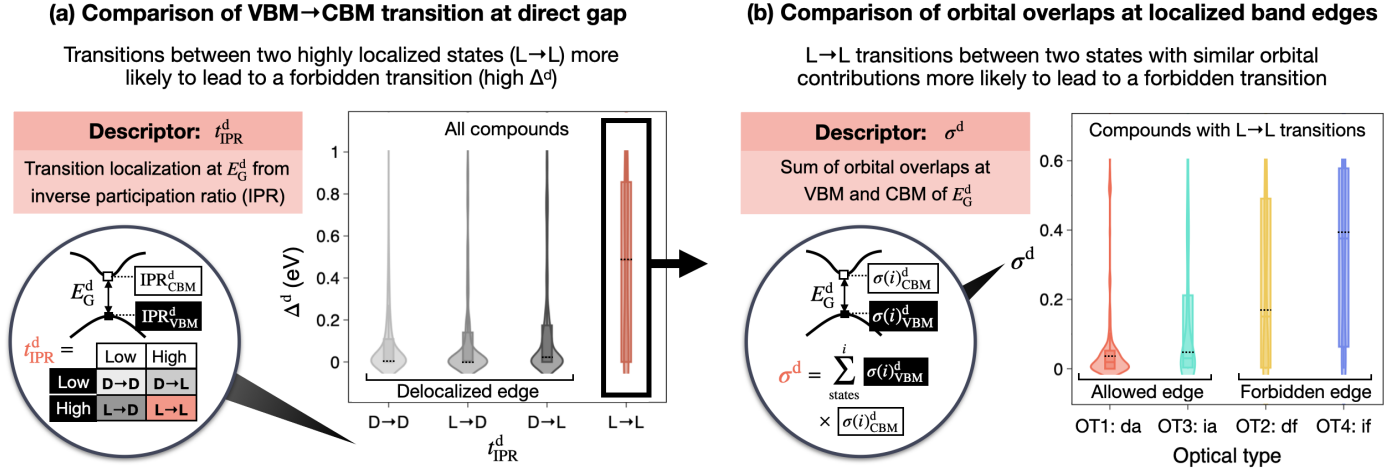


Figure 5: A schematic of band edge orbital descriptors and violin plots correlating each descriptor to the forbidden transitions data set for (a) t_{IPR}^d , the transition localization at the VBM and CBM from the inverse participation ratio (IPR) and (b) $\Sigma\sigma^d$, the orbital overlap of the VBM and CBM states at E_G^d . In (a), “D” indicates a delocalized state and “L” indicates a localized state, and the scenario in which there are transitions from a highly localized state at the VBM to another highly localized state at the CBM (L→L) is highlighted. In (b), only compounds with L→L are plotted, and the violin plot shows the distribution of $\Sigma\sigma^d$ across different optical types (note that OT2 and OT4 indicate forbidden transitions, i.e., $\Delta^d > 0$ eV.) In both violin plots, mean values of each distribution are reported with dashed black lines.

Table I: Most promising predicted TC compounds with forbidden optical transitions (see columns Δ^d and Δ_{edge}^d), and a summary of their computed optical and electronic properties. See SM for full table.

Material ID (mpid)	Formula	Space group	E_{hull} (eV/at.) [†]	E_G (eV) [†]	E_G (eV) [‡]	E_G^d (eV) [‡]	E_G^{da} (eV) [¶]	E_{edge} (eV) [¶]	Δ^d (eV) [†]	Δ_{edge}^d (eV) [¶]	$\bar{\alpha}_{\text{vis}}$ (cm ⁻¹) [¶]	m_e^*	m_h^*	Doping (defects) [†]	# ICSD entries
mp-1009085	BeSiP ₂	$I\bar{4}2d$	0.000	1.15	1.84	1.84	3.04	2.78	1.20	0.94	7.1×10^3	0.35	0.47	p&n	2
mp-9268	KSe	$P\bar{6}2m$	0.000	0.72	1.66	2.14	2.14	3.31	0.00	1.17	4.8×10^3	0.33	1.73	p&n	1
mp-11583	Zr ₂ SN ₂	$P6_3/mmc$	0.000	0.56	1.45	2.65	3.06	2.76	0.41	0.24	8.3×10^3	0.41	0.44	p&n	1
mp-984718	BAs	$P6_3mc$	0.090	1.15	1.82	2.72	3.23	3.05	0.51	0.32	4.6×10^3	0.28	0.38	p-type	0
mp-947	Au ₂ S	$Pn\bar{3}m$	0.000	1.91	3.00	3.00	3.30	3.14	0.30	0.13	3.4×10^3	0.42	1.55	p-type	2
mp-32780	AuCl	$I4_1/amd$	0.000	1.93	3.04	3.04	3.26	3.39	0.23	0.35	1.9×10^3	1.13	0.91	p-type	2
mp-1072104	GeO ₂	$Pnmm$	0.006	1.40	3.23	3.23	3.38	4.02	0.15	0.79	2.2×10^2	0.19	1.62	n-type	6
mp-1224786	GaSbO ₄	$Cmmm$	0.000	0.80	2.47	2.47	2.83	3.34	0.36	0.87	7.7×10^2	0.16	1.45	n-type	0
mp-16293	KSbO ₃	$F\bar{d}3m$	0.045	1.12	2.58	2.89	3.35	3.32	0.46	0.43	1.0×10^3	0.24	0.34	n-type	1
mp-1106089	Ba ₂ InGaO ₅	$Ima2$	0.000	1.42	2.68	2.69	3.27	3.39	0.59	0.71	1.1×10^3	0.22	0.77	n-type	1
mp-1029868	Sr ₅ (SiN ₃) ₂	$C12/c1$	0.000	1.41	2.43	2.59	2.90	3.02	0.31	0.43	3.7×10^3	0.34	1.20	n-type	0
mp-856	SnO ₂	$P4_2/mnm$	0.000	0.66	2.33	2.33	3.06	3.20	0.74	0.87	1.0×10^3	0.14	1.56	n (ref.)	42
mp-22598	In ₂ O ₃	$Ia\bar{3}$	0.000	0.93	2.34	2.34	2.56	3.02	0.22	0.68	2.7×10^3	0.13	6.44	n (ref.)	18

[†]GGA calculations. [‡]HSE06 calculations. [¶]GGA calculations with HSE06 gap correction.

Screen 2: Medium-throughput HSE calculations

In screen 2, band gap refinement calculations are applied to the outputs of screen 1 to better approximate direct allowed gap and the absorption coefficient. This approach assumes that the GGA forbidden energy difference Δ^d is a sufficient proxy for the difference between HSE E_G^d and HSE E_G^{da} ; however this has not been benchmarked to our knowledge, and Δ^d may scale differently depending on functional. Using these HSE shifted energies and spectra, compounds are filtered that fulfill at least one of three criteria as proxies for transparency, as shown in Figure 2: $E_G^{\text{da}} \geq 2.9$ eV, $E_{\text{edge}} \geq 2.9$ eV, or $\bar{\alpha}_{\text{vis}}$ less than that of ITO (2.7×10^3 cm⁻¹). Outputs are reported in Figure 4(c) and (d), yielding 184 previously excluded p-type TC candidates and 243 previously excluded n-type TC candidates.

At this stage, the BPE ratio σ_{BPE} is also computed as a

guideline for whether dopability may be possible. Specifically, BPE energies that lie in the upper quartile of the band gap near the conduction band minimum (CBM; i.e., $\sigma_{\text{BPE}} > 0.75$) have been shown to correlate with unlikely p-type dopability, whereas BPE energies that lie in the lower quartile of the band gap near the valence band maximum (VBM; i.e., $\sigma_{\text{BPE}} < 0.25$) have been shown to correlate negatively with n-type dopability.[25] Therefore, we restrict defect calculations in screen 3 to compounds with $\sigma_{\text{BPE}} < 0.75$ for p-type candidates and $\sigma_{\text{BPE}} > 0.25$ for n-type candidates. Most compounds have mid-gap BPEs so are not excluded from either set. We emphasize that this metric is a guideline that has been demonstrated to correlate with dopability, *not* to predict it, so screens based on BPE should be used with caution.[25]

Top candidates with possible* dopability

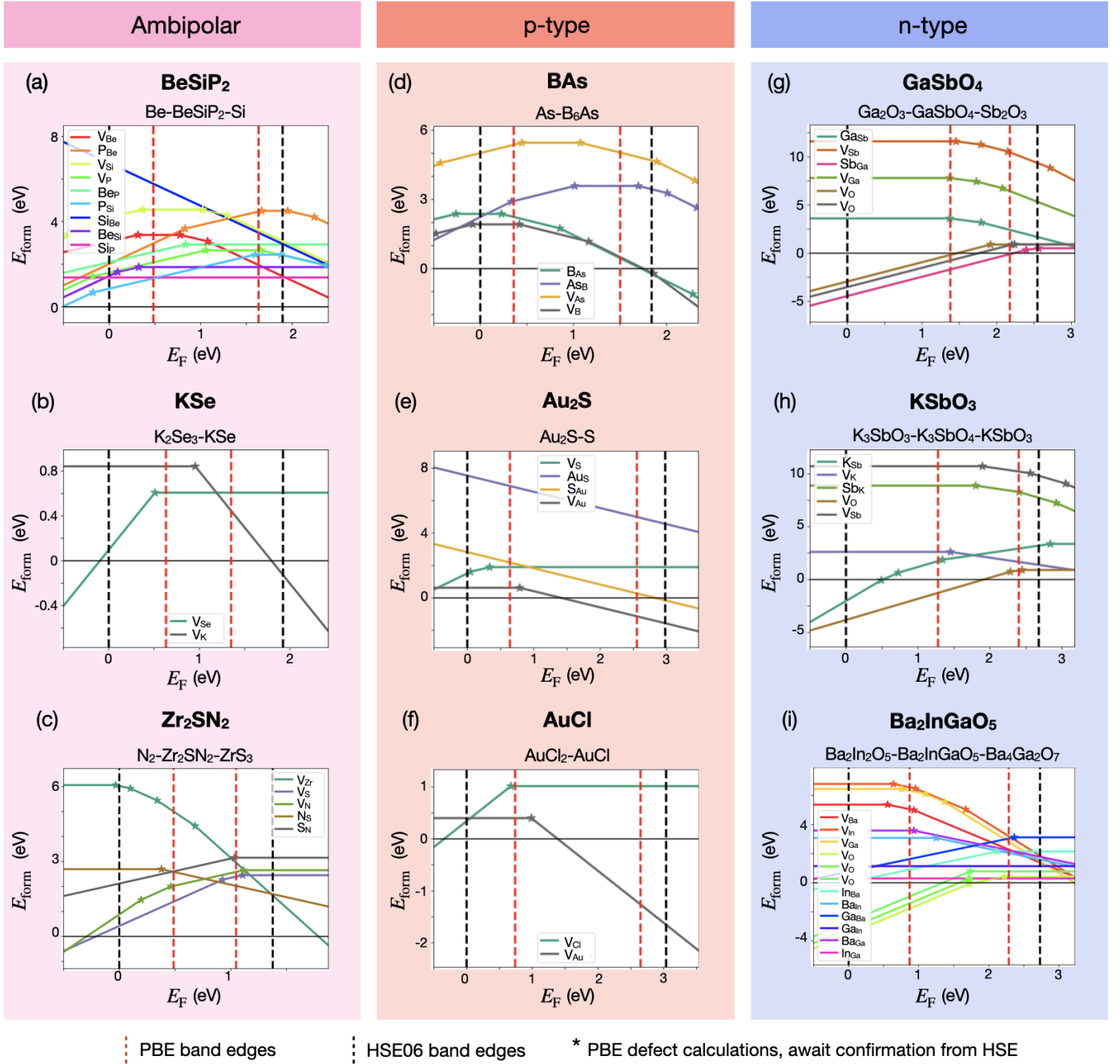


Figure 6: PBE defect formation energy diagrams for a representative set of (a,b,c) candidate ambipolar dopable TCs, (d,e,f) candidate p-type TCs, and (g,h,i) candidate n-type TCs. For each material, only a single representative chemical potential condition is plotted (see SM for other conditions). The KSe diagram plotted here is for K_2Se_3 -KSe and depicts p-type dopability, whereas n-type dopability is computed at a different chemical potential condition (K_2Se -KSe; see SM). We highlight that these are PBE defect calculations (with an HSE band edge “correction”[23]), and await confirmation of dopability from higher levels of theory.

Screen 3: Low-throughput defect and mobility calculations

In the final screening step, GGA defect formation energy calculations are performed (with HSE VBM and CBM corrections[23]) to assess accessible intrinsic carrier concentrations on ~ 100 of the most interesting TC candidates to emerge from screen 2. Many of these compounds have unstable defects or intrinsic pinning defects such that they

are likely not highly dopable (some may be extrinsically dopable, although this has not been investigated here). We identify a subset of compounds with promising dopability, summarized in **Table I** and **Figure 6**. We will refer to these materials herein as “candidates”, as each has shown the potential for dopability, but true dopability remains to be confirmed using higher levels of theory and, for instance, hybrid functionals.

First, our predicted p-type dopable TC candidates include BeSiP_2 , KSe , Zr_2SN_2 , BAs (metastable polymorph with space group $P6_3mc$), Au_2S , and AuCl . All except BAs are on the convex hull and have been synthesized as bulk materials, while the latter two Au_2S and AuCl have been synthesized as thin films. Au_2S is a known p-type semiconductor,[26] and the dopability of AuCl is unknown. BAs is a metastable polymorph with space group $P6_3mc$ (its stable cubic polymorph has had recent attention due to its high thermal conductivity[27, 28], and exhibits p-type conductivity[29]). Compounds KAlTe_2 , $\text{Cd}_3(\text{BO}_3)_2$, ScIO , and KCuO are potentially p-type dopable within a smaller window of tolerance; each have been synthesized in bulk but not thin film form. Defect calculations of ScIO (and KCuO) suggested hole-killing behavior, but only limited chemical potentials were assessed.[30] A few of p-type candidates appear also n-type dopable at various conditions — BeSiP_2 , Zr_2SN_2 , and KSe (at $\text{K}_2\text{Se-KSe}$, see SM) — and therefore may be ambipolar dopable semiconductors, however in each case this remains to be confirmed experimentally. We highlight the variety of non-oxide chemistries emerging here; typically forbidden transitions have been studied in oxides, but we demonstrate the importance of looking beyond oxides. In chalcogenides reported here, p-type dopability is limited by anion vacancies.

Compounds in which defects suggest candidate n-type TCs include rutile GeO_2 , GaSbO_4 , KSbO_3 , $\text{Ba}_2\text{InGaO}_5$, $\text{Sr}_5(\text{SiN}_3)_2$, and LiYS_2 (as well as ambipolar candidates BeSiP_2 , KSe , and Zr_2SN_2), while Rb_2SnBr_6 , $\text{Sr}(\text{YS}_2)_2$, and GaBiO_3 are potentially n-type dopable within a smaller window of tolerance (see SM). Many of these outputs corroborate literature findings. Notably, the two highest-performing, commercially-available n-type TCs — In_2O_3 and SnO_2 — emerge from the screening at this stage; both have $\Delta^d > 0$ eV, and we also include them in Table I for reference. This is important, as the use of screening parameters from previous studies would have filtered out the best TCs, likely due to their low GGA band gaps (0.66 and 0.93, respectively) and the presence of forbidden transition states at the band edges.[25] Rutile GeO_2 has been recently studied as an ultra-wide-band-gap material and has been shown to be experimentally ambipolar dopable,[31, 32] while GeO_2 -derived germanates (e.g., SrGeO_3) have been explored as n-type TCOs.[33] Sb-based GaSbO_4 has been explored preliminarily as an n-type TCO.[34] Perovskite Rb_2SnBr_6 has been recently confirmed experimentally as n-type but not yet studied as a TC[35], while SrY_2S_4 has been grown as a thin film but doping not confirmed. To our knowledge $\text{Ba}_2\text{GaInO}_5$ has been grown in bulk but not thin film form [36] (a similar compound, brownmillerite $\text{Ba}_2\text{In}_2\text{O}_5$, has shown both n-type and p-type doping and ionic conductivity[37]). All reported oxides are in the main group, corroborating literature consensus on conditions for low effective mass in TCOs;[10] we report several non-oxides here, but in each case m_e^* is not as high as in oxides.

To assess charge transport, the mobilities of a few representative candidates are computed using the `amset`

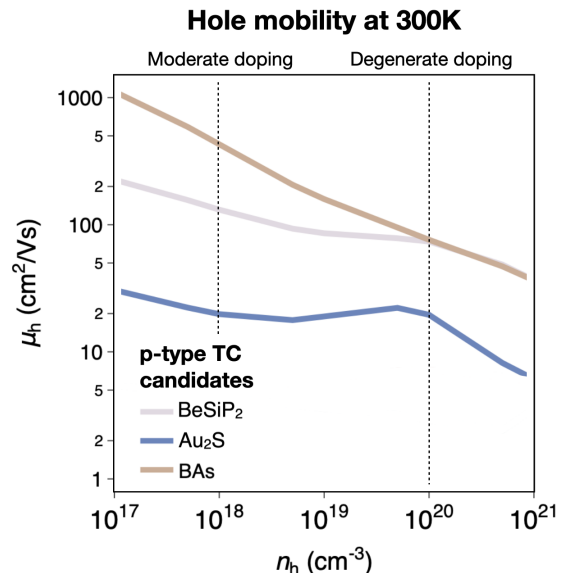


Figure 7: Hole mobility μ_h computed with `amset` code for a representative subset of p-type TC candidates, as a function of doping concentration n_h . See SM for electron mobility calculations.

package.[38] As shown in **Figure 7**, of these compounds, high hole computed mobilities μ_h (greater than $10 \text{ cm}^2/\text{Vs}$ at 300 K at both moderate and degenerate dopings) are exhibited in BeSiP_2 , BAs, and Au_2S , with the former two exhibiting $\mu_h > 100 \text{ cm}^2/\text{Vs}$. BeSiP_2 also has a computed electron mobility μ_e higher than that of standards of In_2O_3 and SnO_2 , as shown in the SM. Computed mobilities incorporate polar optical phonon, ionized impurity, and acoustic deformation potential scattering modes. These calculations can be interpreted as an upper limit for scattering in high quality thin films; we do not assess grain-boundary scattering, which is common in thin films.

To confirm dopability in the two most promising p-type TCs to emerge from the screening — BeSiP_2 and BAs — hybrid defect calculations are performed, as summarized in the SM. These calculations corroborate the PBE defect calculations, suggesting ambipolar dopability in BeSiP_2 (limited by phosphorus vacancies V_P for p-type doping and beryllium vacancies V_{Be} for n-type doping) and p-type dopability BAs (limited by boron vacancies, V_B).

Identification of candidate TCs with forbidden transitions

Here, we summarize the optical and electronic properties of the most promising candidates to emerge from GGA defect calculations, as reported in Table I, and highlight a few examples. Each emerging compound has a GGA gap E_G below 2 eV, but either an HSE-corrected E_G^{da} or E_{edge} greater than 3 eV due to the presence of forbidden transitions or a high Δ_{edge}^d . Au_2S , AuCl , and GeO_2 have HSE gaps E_G greater than 3 eV so may have emerged from previous screenings but are included here due to their forbidden transitions; KSe does not have forbidden tran-

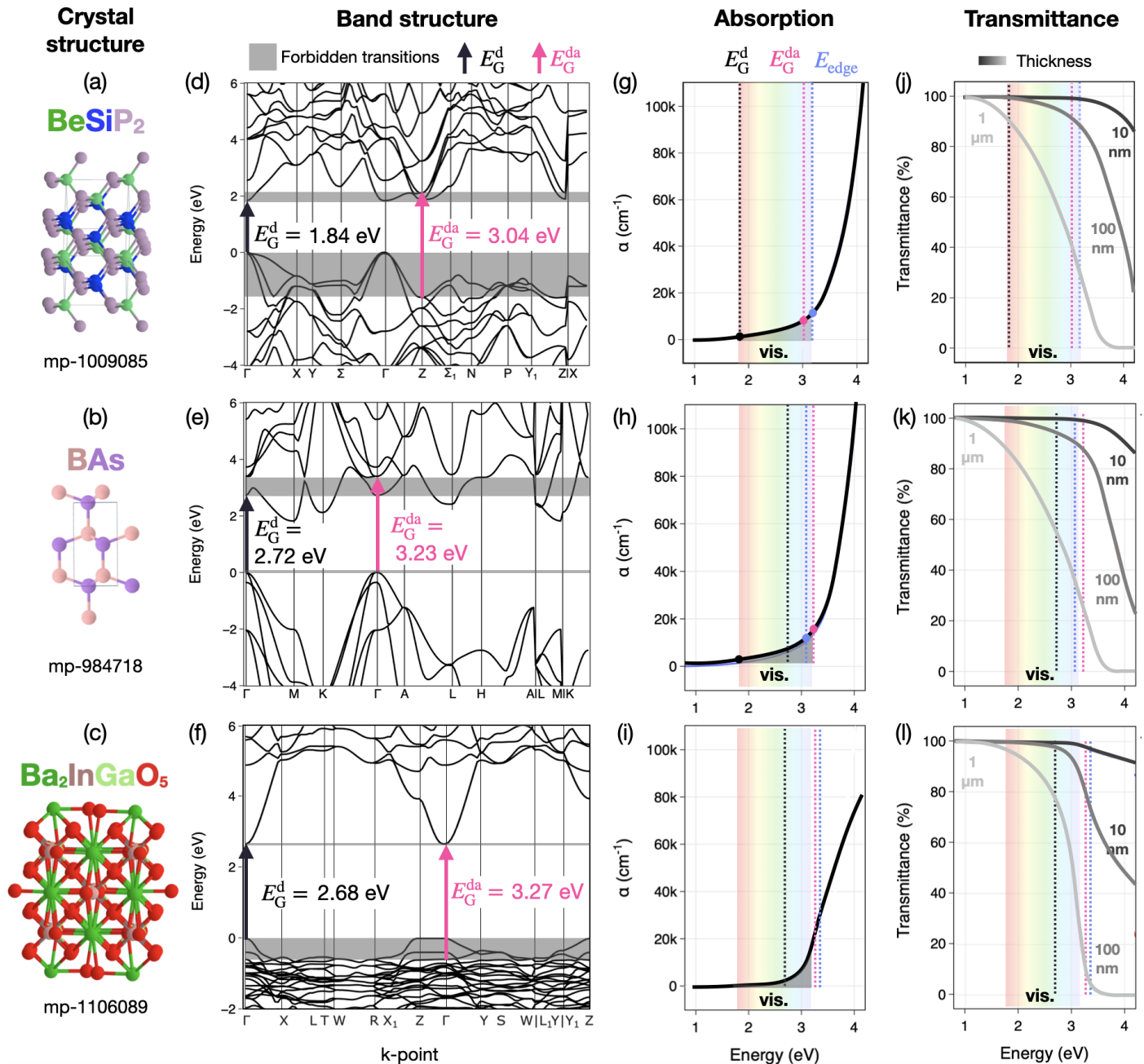


Figure 8: (a–c) Crystal structure, (d–f) HSE-corrected electronic band diagram, (g–i) computed absorption coefficient, and (j–l) computed transmittance for three representative candidates from our screening with forbidden optical transitions: ambipolar-dopable BeSiP₂, p-type dopable BAs, and n-type dopable Ba₂InGaO₅. HSE direct and direct allowed gaps E_G^d and E_G^{da} are denoted with black and pink lines, respectively, and in (b) grey shading indicates the region in which optical transitions are forbidden between the VB and CB states. Rainbow shading in (c) and (d) corresponds the visible spectrum (“vis.”).

sitions, but Δ_{edge}^d is greater than 1 eV so it is included as well. Compounds in which $\bar{\alpha}_{\text{vis}}$ is less than that of In₂O₃ and likely exhibit a high degree of transparency are GeO₂, AuCl, KSbO₃, and Ba₂InGaO₅. The former has been investigated in depth, but the latter three would be particularly interesting candidates for follow-up studies.

In **Figure 8** we (a–c) highlight crystal structure and (d–l) optical properties for candidates chalcopyrite BeSiP₂ and wurtzite BAs, selected as representative materials since charge transport and hybrid defect calculations have confirmed p-type dopability and mobility, as well as pre-

dicted brownmillerite Ba₂InGaO₅ as an n-type example. The electronic band structure diagrams of BeSiP₂ (d), BAs (e), and Ba₂InGaO₅ (f) demonstrate that the direct allowed gap E_G^{da} (pink arrow) is larger than E_G^d (black arrow), and the band extrema at Γ are very disperse, which leads to low effective masses and high mobilities. The grey shading depict regions in which optical transitions are forbidden. For example, in Ba₂InGaO₅ (f) transitions between the upper two VBs along the Γ -X, Γ -Y, Γ -Z paths, as well as the L-T-W path, are forbidden. Thus, the third-highest VB is the highest VB at which transitions between

the CBM are allowed, and $E_G^{\text{da,HSE}}$ occurs at the Γ -point at approximately -0.6 eV. These examples demonstrate three different scenarios in which forbidden transitions can occur. In $\text{Ba}_2\text{InGaO}_5$ the E_G^{da} and E_G^{d} occur at the same k-point (Γ) and states are forbidden at the VBM, in BAs the E_G^{da} and E_G^{d} occur at the same k-point (Γ) and states are forbidden at the CBM, while in BeSiP_2 E_G^{da} occurs at a different k-point (Z) than E_G^{d} (Γ) and states are forbidden both at the VBM and the CBM.

Panels (g-i) show HSE-corrected absorption coefficient as a function of photon energy, with the edge energy difference E_{edge} denoted. In each example material, E_{edge} are within a few tens of meV of E_G^{da} , although in other candidates this is not necessarily the case (see Table I, e.g., In_2O_3). Importantly, in both cases E_{edge} is at the violet edge of the visible spectrum, which indicates a likelihood of transparency in the visible. Panels (j-k) report transmittance from the Beer-Lambert law (see SM), and the color of the trace corresponds to the thickness of a thin film. As expected, thinner films are more transparent, however the decrease in transparency as thickness increases is material-dependent. For example, although both BeSiP_2 and $\text{Ba}_2\text{InGaO}_5$ have >99% transmittance for 10 nm thick films, 1 μm thick films of $\text{Ba}_2\text{InGaO}_5$ have a T_{vis} of $\sim 75\%$ while T_{vis} drops to less than 50% in BeSiP_2 . However, although BeSiP_2 has >99% transmittance for 10 nm thick films, T_{vis} drops to less than 50% in 1 μm thick films. Therefore this metric is important when selecting materials for real device applications.

DISCUSSION

Synthesis considerations

So far we have used simulations to predict properties; the next step for the TC community is to synthesize these materials as thin films and assess their properties experimentally. The final column of Table I reports the number of experimental ICSD database entries, showing all but four (BAs, $\text{Sr}_5(\text{SiN}_3)_2$, AlSbO_4 , LiYS_2) have been previously synthesized (although AlSbO_4 has been recently reported[34]). However in many compounds with ICSD entries, thin films have not yet been grown nor characterized and dopability has not been assessed experimentally (e.g., BeSiP_2 , KSe , $\text{Ba}_2\text{InGaO}_5$, KAlTe_2 , ScIO , KCuO , etc.).

Some of our candidates have known synthesis challenges, in particular since thin film synthesis is often at non-equilibrium conditions and presents other difficulties. In perovskite oxides KSbO_3 and GaBiO_3 low m_e^* has been highlighted[10] but phase-pure thin film synthesis has proven challenging so doping remains to be confirmed.[39] Non-oxide chalcogenides yield particular synthesis barriers due to decomposition: KSe has not been synthesized as a thin film to our knowledge, and KAlTe_2 is likely challenging to synthesize due to oxidation. For candidates that do not have ICSD entries, synthesis may have been attempted

but was not successful for various reasons. Wurtzite BAs has been challenging to crystallize and has not yet been synthesized as a thin film to our knowledge; it is similar in chemistry to zincblende BP, which was predicted computationally as a p-type TC[18] and has since been synthesized as a thin film.[40]

We acknowledge that some of these candidates are also likely not practical or safe to scale up into device applications. In particular, Be and Be-containing compounds are toxic to humans and the environment,[41] so although BeSiP_2 has been synthesized it is most likely not a practical TC material. However, since this compound has a common chalcopyrite crystal structure with a small unit cell, understanding the physics behind its large forbidden transition and disperse valence band is demonstrative and could inspire design criteria of other p-type TCs (see Figure 8).

Challenges and context

From the set of 18,000 materials with absorption calculations, we have proposed a set of TC candidates with forbidden optical transitions at their band edges and plausible dopability and high mobility. There is a general correlation across all semiconductors that, as the fundamental electronic gap increases, doping becomes more challenging and band edges become less disperse.[42, 43] Previous searches for p-type TCs have endeavored to identify cases in which a single state at the VBM is both disperse over k-space and facilitates transitions which lead to a wide gap. In contrast, by decoupling these two parameters such that allowed transitions do not need to occur at the band edge, our metric could enable better electronic properties while the optical gap is widened. One challenge with this design metric is that localized band edges, which we have shown to correlate with forbidden transitions, tend to lead to *higher* effective masses and therefore lower mobilities. However, we have also demonstrated many candidate TCs with delocalized band edges and forbidden transitions.

The absorption spectra we have computed are first-order, high-throughput approximations, and therefore interpretation of results must consider their limitations. We do not include the effects of spin-orbit coupling, which may influence the orbital character of the band edges or induce spin-forbidden transitions. The IPA accounts only for interband absorption at a fixed k-point, and therefore intraband absorption matrix elements are not considered (phonon-assisted transitions such as indirect gap). This may be sufficient for a first-order approximation since indirect absorption tends to be weak, but in heavily doped TCs, strong free-carrier absorption can arise due to intraband transitions.[44]. Off-stoichiometries and dopants can also introduce shallow defect levels within the gap that reduce optical transparency, and absorption from excitons may also become significant at energies just below the fundamental absorption edge, leading to a reduction of transparency.[44] Despite these limitations, our calcula-

tions and data have added information and improved design metrics towards furthering the search for novel TCs.

CONCLUSION

In this study, we have described the absorption edge and optical type for $\sim 18,000$ semiconductors in the Materials Project database, and we have shared this data publicly on the MPContribs platform. Using a set of descriptors for absorption and orbital character, we have demonstrated correlations between the presence of forbidden optical transitions, localized band edges, and orbital overlap. From this set of materials, we have screened for n-type or p-type TC materials, and propose a set of candidates with forbidden band edge transitions and promising optical and electronic properties such as chalcopyrite BeSiP_2 and wurtzite BAs. Notably, high-performance TCs such as ITO emerge from this screening, while being excluded from those based on the fundamental gap alone. Since over half of the set of $\sim 18,000$ semiconductors have forbidden optical transitions at their band edges (OT2 or OT4), we recommend that future high-throughput screenings for optical properties use metrics representative of absorption spectra rather than band gap alone.

ACKNOWLEDGEMENTS

This work was supported by the U.S. Department of Energy, Office of Science, Office of Basic Energy Sciences, Materials Sciences and Engineering Division under Contract No. DE-AC02-05-CH11231 (Materials Project program KC23MP). R.W.R. was supported by the U.C. Berkeley Chancellor’s Fellowship and the National Science Foundation (NSF) Graduate Research Fellowship under Grant No. DGE1106400 and DGE175814. A.M.G. was supported by EPSRC Fellowship EP/T033231/1. We acknowledge compute resources from National Energy Research Scientific Computing Center (NERSC), a DOE Office of Science User Facility. We thank Doug Fabini for helpful discussions, and Ruoxi Yang, Jason Munro, and David Mrdjenovich for fruitful discussion and insights.

AUTHOR CONTRIBUTIONS

R.W.R.: Conceptualization, Methodology, Coding, Computational Investigation, Writing - Original Draft, Writing - Review & Editing, Funding Acquisition; Y.X.: Computational Investigation (PBE defect formation energy calculations); J.X.S.: Supervision, Coding; M.K.H.: Supervision, Methodology, Coding; N.W.: Computational Investigation (HSE defect formation energy calculations); M.A.: Funding Acquisition, Resources, Supervision; A.G.: Computational Investigation (amset calculations); G.H.: Conceptualization, Supervision, Writing - Review & Editing; K.A.P.: Funding Acquisition, Project Administration, Resources, Supervision, Writing - Review & Editing.

REFERENCES

- [1] L. Yu and A. Zunger, “Identification of potential photovoltaic absorbers based on first-principles spectroscopic screening of materials,” *Physical Review Letters*, vol. 108, no. 6, p. 068701, 2012.
- [2] A. Walsh, J. L. Da Silva, S.-H. Wei, C. Körber, A. Klein, L. Piper, A. DeMasi, K. E. Smith, G. Panaccione, P. Torelli, *et al.*, “Nature of the band gap of In_2O_3 revealed by first-principles calculations and x-ray spectroscopy,” *Physical Review Letters*, vol. 100, no. 16, p. 167402, 2008.
- [3] R. Summitt, J. A. Marley, and N. F. Borrelli, “The ultraviolet absorption edge of stannic oxide (SnO_2),” *Journal of Physics and Chemistry of Solids*, vol. 25, no. 12, pp. 1465–1469, 1964.
- [4] D. Fröhlich, R. Kenklies, and R. Helbig, “Band-gap assignment in SnO_2 by two-photon spectroscopy,” *Physical Review Letters*, vol. 41, no. 25, p. 1750, 1978.
- [5] D. Segev and S.-H. Wei, “Structure-derived electronic and optical properties of transparent conducting oxides,” *Physical Review B*, vol. 71, no. 12, p. 125129, 2005.
- [6] A. B. Kehoe, D. O. Scanlon, and G. W. Watson, “Nature of the band gap of Tl_2O_3 ,” *Physical Review B*, vol. 83, no. 23, p. 233202, 2011.
- [7] H. Tang, H. Berger, P. Schmid, and F. Levy, “Optical properties of anatase (TiO_2),” *Solid State Communications*, vol. 92, no. 3, pp. 267–271, 1994.
- [8] X. Nie, S.-H. Wei, and S. Zhang, “Bipolar doping and band-gap anomalies in delafossite transparent conductive oxides,” *Physical Review Letters*, vol. 88, no. 6, p. 066405, 2002.
- [9] G. Hautier, A. Miglio, G. Ceder, G.-M. Rignanese, and X. Gonze, “Identification and design principles of low hole effective mass p-type transparent conducting oxides,” vol. 4, p. 2292.
- [10] G. Hautier, A. Miglio, D. Waroquiers, G.-M. Rignanese, and X. Gonze, “How does chemistry influence electron effective mass in oxides? a high-throughput computational analysis,” *Chemistry of Materials*, vol. 26, no. 19, pp. 5447–5458, 2014.
- [11] A. Bhatia, G. Hautier, T. Nilgianskul, A. Miglio, J. Sun, H. J. Kim, K. H. Kim, S. Chen, G.-M. Rignanese, X. Gonze, and J. Suntivich, “High-mobility bismuth-based transparent p-Type oxide from high-throughput material screening,” vol. 28, no. 1, pp. 30–34.
- [12] V.-A. Ha, G. Yu, F. R. Ricci, D. Diana, M. J. V. Setten, M. Giantomassi, G.-M. Rignanese, and G. Hautier, “Computationally-driven, high throughput identification of CaTe and Li_3Sb as promising candidates for high mobility p-Type transparent conducting materials,” vol. 3, no. 3, p. 34601.
- [13] G. Brunin, F. Ricci, V.-A. Ha, G.-M. Rignanese, and G. Hautier, “Transparent conducting materials discovery using high-throughput computing,” *npj Computational Materials*, vol. 5, no. 1, p. 63, 2019.
- [14] A. J. Jackson, B. J. Parrett, J. Willis, A. M. Ganose, W. W. Leung, Y. Liu, B. A. Williamson, T. K. Kim, M. Hoesch, L. S. Veiga, *et al.*, “Computational prediction and experimental realization of earth-abundant transparent conducting oxide Ga -doped ZnSb_2O_6 ,” *ACS Energy Letters*, vol. 7, no. 11, pp. 3807–3816, 2022.
- [15] N. Sarmadian, R. Saniz, B. Partoens, and D. Lamoen, “Easily doped p-type, low hole effective mass, transparent oxides,” vol. 6, pp. 1–9.
- [16] B. A. D. Williamson, J. Buckeridge, J. Brown, S. Ansbro, R. G. Palgrave, and D. O. Scanlon, “Engineering valence

- band dispersion for high mobility p-type semiconductors,” vol. 29, no. 6, pp. 2402–2413.
- [17] J. Shi, T. F. Cerqueira, W. Cui, F. Nogueira, S. Botti, and M. A. Marques, “High-throughput search of ternary chalcogenides for p-Type transparent electrodes,” vol. 7, pp. 1–13.
 - [18] J. B. Varley, A. Miglio, V. A. Ha, M. J. V. Setten, G. M. Rignanese, and G. Hautier, “High-throughput design of non-oxide p-type transparent conducting materials: Data mining, search strategy, and identification of boron phosphide,” vol. 29, no. 6, pp. 2568–2573.
 - [19] W. Meng, X. Wang, Z. Xiao, J. Wang, D. B. Mitzi, and Y. Yan, “Parity-forbidden transitions and their impact on the optical absorption properties of lead-free metal halide perovskites and double perovskites,” *Journal of Physical Chemistry Letters*, vol. 8, no. 13, pp. 2999–3007, 2017.
 - [20] D. H. Fabini, M. Koerner, and R. Seshadri, “Candidate inorganic photovoltaic materials from electronic structure-based optical absorption and charge transport proxies,” *Chemistry of Materials*, vol. 31, no. 5, pp. 1561–1574, 2019.
 - [21] Á. Morales-García, R. Valero, and F. Illas, “An empirical, yet practical way to predict the band gap in solids by using density functional band structure calculations,” *The Journal of Physical Chemistry C*, vol. 121, no. 34, pp. 18862–18866, 2017.
 - [22] P. Y. Yu and M. Cardona, *Fundamentals of semiconductors*. Elsevier, 4 ed., 2005.
 - [23] D. Broberg, K. Bystrom, S. Srivastava, D. Dahliah, B. A. D. Williamson, L. Weston, D. O. Scanlon, G.-M. Rignanese, S. Dwaraknath, J. Varley, K. A. Persson, M. Asta, and G. Hautier, “High-throughput calculations of charged point defect properties with semi-local density functional theory - performance benchmarks for materials screening applications,” *npj Computational Materials*, 2023.
 - [24] M. Chan and G. Ceder, “Efficient band gap prediction for solids,” *Phys. Rev. Letters*, vol. 105, no. 19, p. 196403, 2010.
 - [25] R. Woods-Robinson, D. Broberg, A. Faghaninia, A. Jain, S. S. Dwaraknath, and K. A. Persson, “Assessing high-throughput descriptors for prediction of transparent conductors,” vol. 30, no. 22, pp. 8375–8389.
 - [26] K. Ishikawa, T. Isonaga, S. Wakita, and Y. Suzuki, “Structure and electrical properties of Au_2S ,” *Solid State Ionics*, vol. 79, pp. 60–66, 1995.
 - [27] L. Lindsay, D. Broide, and T. Reinecke, “First-principles determination of ultrahigh thermal conductivity of boron arsenide: A competitor for diamond?,” *Physical review letters*, vol. 111, no. 2, p. 025901, 2013.
 - [28] J. S. Kang, M. Li, H. Wu, H. Nguyen, and Y. Hu, “Experimental observation of high thermal conductivity in boron arsenide,” *Science*, vol. 361, no. 6402, pp. 575–578, 2018.
 - [29] J. L. Lyons, J. B. Varley, E. R. Glaser, J. A. Freitas Jr, J. C. Culbertson, F. Tian, G. A. Gamage, H. Sun, H. Ziyadee, and Z. Ren, “Impurity-derived p-type conductivity in cubic boron arsenide,” *Applied Physics Letters*, vol. 113, no. 25, p. 251902, 2018.
 - [30] H. Wiebeler, R. K. M. Raghupathy, H. Mirhosseini, and T. D. Kühne, “Virtual screening of nitrogen-, phosphorous- and halide-containing materials as p-type transparent conductors,” *Journal of Physics: Materials*, vol. 4, no. 1, p. 015004, 2020.
 - [31] S. Chae, J. Lee, K. A. Mengle, J. T. Heron, and E. Kioupakis, “Rutile geo_2 : an ultrawide-band-gap semiconductor with ambipolar doping,” *Applied Physics Letters*, vol. 114, no. 10, p. 102104, 2019.
 - [32] S. Chae, K. Mengle, K. Bushick, J. Lee, N. Sanders, Z. Deng, Z. Mi, P. F. Poudeu, H. Paik, J. T. Heron, *et al.*, “Toward the predictive discovery of ambipolarly dopable ultra-wide-band-gap semiconductors: The case of rutile geo_2 ,” *Applied Physics Letters*, vol. 118, no. 26, p. 260501, 2021.
 - [33] H. Mizoguchi, T. Kamiya, S. Matsuishi, and H. Hosono, “A mizoguchiite transparent conductive oxide,” *Nature communications*, vol. 2, no. 1, p. 470, 2011.
 - [34] W. W. Leung, *Synthesis and characterisation of Group 15-containing inorganic solids for energy conversion applications*. PhD thesis, UCL (University College London), 2020.
 - [35] R. Ganesan, S. Vinodhini, R. Arulmozhi, and R. Muralidharan, “Influence of halogen substitution in double perovskite $\text{Rb}_2\text{Sn}(\text{BrO}_3)_6$ on the photocatalytic degradation of methylene blue dye under visible light irradiation,” *Journal of Materials Science: Materials in Electronics*, vol. 34, no. 2, p. 151, 2023.
 - [36] C. Didier, J. Claridge, and M. Rosseinsky, “Crystal structure of brownmillerite $\text{Ba}_2\text{In}_2\text{O}_5$,” *Journal of Solid State Chemistry*, vol. 218, pp. 38–43, 2014.
 - [37] C. Fisher and M. Islam, “Defect, protons and conductivity in brownmillerite-structured $\text{Ba}_2\text{In}_2\text{O}_5$,” *Solid State Ionics*, vol. 118, no. 3-4, pp. 355–363, 1999.
 - [38] A. M. Ganose, J. Park, A. Faghaninia, R. Woods-Robinson, K. A. Persson, and A. Jain, “Efficient calculation of carrier scattering rates from first principles,” *Nature communications*, vol. 12, no. 1, pp. 1–9, 2021.
 - [39] R. Homcheunjit, P. Pluengphon, A. Tubtimtae, and P. Teetsopon, “Structural, optical, and electrical properties via two simple routes for the synthesis of multiphase potassium antimony oxide thin films,” *Physica B: Condensed Matter*, vol. 637, p. 413885, 2022.
 - [40] A. Crovetto, J. M. Adamczyk, R. R. Schnepf, C. L. Perkins, H. Hempel, S. R. Bauers, E. S. Toberer, A. C. Tamboli, T. Unold, and A. Zakutayev, “Boron phosphide films by reactive sputtering: Searching for a p-type transparent conductor,” *Advanced Materials Interfaces*, vol. 9, no. 12, p. 2200031, 2022.
 - [41] C. Smith, L. Ingerman, and R. Amata, “Toxicological profile for beryllium,” 2002.
 - [42] A. Zunger, “Practical doping principles,” vol. 83, no. 1, p. 57.
 - [43] C. Kittel and B. Kittel, *Introduction to Solid State Physics*, vol. 8. Wiley.
 - [44] J. I. Pankove, *Optical Processes in Semiconductors*. Courier Corporation.
 - [45] P. E. Blöchl, “Projector augmented-wave method,” vol. 50, no. 24, p. 17953.
 - [46] G. Kresse and D. Joubert, “From ultrasoft pseudopotentials to the projector augmented-wave method,” vol. 59, no. 3, pp. 1758–1775.
 - [47] G. Kresse and J. Hafner, “*Ab initio* molecular dynamics for liquid metals,” vol. 47, no. 1, pp. 558–561.
 - [48] G. Kresse and J. Furthmüller, “Efficient iterative schemes for *ab initio* total-energy calculations using a plane-wave basis set,” vol. 54, no. 16, p. 11169.
 - [49] J. P. Perdew, K. Burke, and M. Ernzerhof, “Generalized gradient approximation made simple,” vol. 77, no. 18, p. 3865.
 - [50] S. P. Ong, W. D. Richards, A. Jain, G. Hautier, M. Kocher, S. Cholia, D. Gunter, V. L. Chevrier, K. A. Persson, and G. Ceder, “Python materials Genomics (pymatgen): A robust, open-source python library for materials analysis,” vol. 68, pp. 314–319.
 - [51] A. Jain, S. P. Ong, G. Hautier, W. Chen, W. D. Richards, S. Dacek, S. Cholia, D. Gunter, D. Skinner, G. Ceder, and K. A. Persson, “Commentary: The Materials Project: A materials genome approach to accelerating materials inno-

- vation,” vol. 1, no. 1, p. 011002.
- [52] G. K. Madsen, J. Carrete, and M. J. Verstraete, “Boltztrap2, a program for interpolating band structures and calculating semi-classical transport coefficients,” *Computer Physics Communications*, vol. 231, pp. 140–145, 2018.
- [53] J. Heyd, G. E. Scuseria, and M. Ernzerhof, “Hybrid functionals based on a screened coulomb potential,” *J. Chem. Phys.*, vol. 118, no. 18, pp. 8207–8215, 2003.
- [54] R. X. Yang, M. K. Horton, J. Munro, and K. A. Persson, “High-throughput optical absorption spectra for inorganic semiconductors,” *arXiv preprint arXiv:2209.02918*, 2022.
- [55] M. Aykol, S. S. Dwaraknath, W. Sun, and K. A. Persson, “Thermodynamic limit for synthesis of metastable inorganic materials,” *Science advances*, vol. 4, no. 4, p. eaaq0148, 2018.
- [56] W. Sun, S. T. Dacek, S. P. Ong, G. Hautier, A. Jain, W. D. Richards, A. C. Gamst, K. A. Persson, and G. Ceder, “The thermodynamic scale of inorganic crystalline metastability,” *Science advances*, vol. 2, no. 11, p. e1600225, 2016.
- [57] P. Huck, D. Gunter, S. Cholia, D. Winston, A. N’Diaye, and K. Persson, “User applications driven by the community contribution framework mpcontributes in the materials project,” *Concurrency and Computation: Practice and Experience*, vol. 28, no. 7, pp. 1982–1993, 2016.
- [58] D. Broberg, B. Medasani, N. E. Zimmermann, G. Yu, A. Canning, M. Haranczyk, M. Asta, and G. Hautier, “Pycdt: A python toolkit for modeling point defects in semiconductors and insulators,” *Computer Physics Communications*, vol. 226, pp. 165–179, 2018.
- [59] J. Hutter, M. Iannuzzi, F. Schiffmann, and J. VandeVondele, “cp2k: atomistic simulations of condensed matter systems,” *Wiley Interdisciplinary Reviews: Computational Molecular Science*, vol. 4, no. 1, pp. 15–25, 2014.
- [60] T. D. Kühne, M. Iannuzzi, M. Del Ben, V. V. Rybkin, P. Seewald, F. Stein, T. Laino, R. Z. Khaliullin, O. Schütt, F. Schiffmann, *et al.*, “Cp2k: An electronic structure and molecular dynamics software package-quickstep: Efficient and accurate electronic structure calculations,” *The Journal of Chemical Physics*, vol. 152, no. 19, p. 194103, 2020.